

Monodimensional effects on elastic and vibrational properties of lacunary networks

Pascal Jean-Michel Monceau and Jean-Claude Serge Levy

Laboratoire de magnétisme des surfaces, Université Paris 7, 2 place Jussieu, 75251 Paris, Cedex 05, France

(Received 18 February 1993)

Elastic and vibrational properties of lacunary square networks with first-neighbor central forces are shown to reduce, in the framework of the harmonic approximation, to longitudinal modes determined by a fragmentation in independent blocks, i.e., segments. Vibrational spectra are thoroughly analyzed with evidence for a transition from continuous spectra to Dirac singularities via singular continuous spectra which occur near the linear percolation threshold. Random lacunary networks, as well as fractal ones, are studied.

I. INTRODUCTION

The study of the properties of materials such as polymers,¹ composites,² and gels has required the extension of the theory of elasticity to disordered and heterogeneous media; in most cases, the classical theory of elasticity of continuous media cannot be generalized in a direct way. Tools and concepts from statistical physics have turned out to be much more fruitful: There is no doubt that theories of percolation and critical phenomena have enabled theorists to take a great step forward³ in this domain. It has been shown, in the case of random networks,⁴ that the critical behavior of macroscopic elastic moduli as a function of the concentration of occupied sites can be described by a percolation transition^{5,6} for different Hamiltonian models, such as the Born one.⁷ A strong reason for percolation effect is that, if there is no link, there is no elasticity. In the case of random square networks with first- and second-neighbor string interactions, it has been shown⁸ that elasticity at rather high density can be described by mean-field theories while near-zero elasticity is well described by percolation effects. The elastic percolation thresholds, as well as the power laws, depend on both the nature of microscopic interactions and geometry.^{8,9} Moreover, it is now well established that the electric and elastic properties of random percolating networks do not belong to the same universality class,¹⁰ except in the particular case of the scalar Born Hamiltonian.

A few studies of elastic properties have been done in the borderline case of nearest-neighbor harmonic interactions, also called central forces, for triangular random lattices⁶ and deterministic Sierpinski gaskets,¹¹ a very few ones⁸ for square and cubic lattices. In the case of the regular Sierpinski gasket, a well-known model for percolation clusters, several authors¹²⁻¹⁴ show that electronic and vibrational spectra exhibit a singular continuous character, i.e., sets of Lebesgue measure zero, with high degeneracies. Furthermore, it is well known that, for cubic lattices, the shear modulus is equal to zero and that the bulk modulus goes to zero when an infinitesimal fraction of bonds is missing.^{6,8} Dealing with a first-neighbor central-force Hamiltonian on a square lattice, we show in this paper that disconnected segments of nearest neigh-

bors are elastically independent at first order; so the small-amplitude vibrations in the plane factor into modes of disconnected linear segments. Thus the elastic and vibrational properties in such materials reduce to a segmentation problem, leading to the notion of linear percolation. It enables us to reach our main purpose: a detailed study of elasticity and vibrational spectra of finite and macroscopic lacunary networks. A basic interest of this work on random networks is the study of vibrational spectra without any recursion formula and the search for general conditions for the occurrence of singular continuous spectra.

Practically, we deal with two kinds of networks.

(i) Bidimensional random square networks $R(n, q)$: q lacunas—each lacuna defined as an unoccupied site—are distributed at random among n^2 possible sites in a square of side $(n-1)a$ and of lattice parameter a . Most of the results set out concerning random square networks are generalized to any space dimension $d > 2$, where q lacunas are distributed among the n^d possible sites of a hypercube of side $(n-1)a$.

(ii) Bidimensional random Sierpinski carpets $C(n, p)$ are constructed according to an iterative process by selecting at random p subsquares among the n^2 possible ones at each level of iteration. Figure 1 shows an example of a finite-size random Sierpinski carpet $C(4, 13)$ at the level $k=4$ of iteration; there are $p^k=13^4$ occupied sites, each one corresponding to an elementary black square; the parameter a of the network is defined as the side of an elementary square. Although deterministic Sierpinski carpets—and gaskets—have been often used as a basic model to represent fractal materials,^{15,16} the statistical scale invariance of random Sierpinski carpets makes them better candidates for the description of such materials. Unfortunately, their random character makes analytical calculations much more difficult.

The central-force Hamiltonian is written as

$$H = \frac{1}{2} k_e \sum (\|(\mathbf{R}_i - \mathbf{R}_j) + (\mathbf{u}_i - \mathbf{u}_j)\| - a)^2 . \quad (1)$$

k_e is an elastic constant, and the summation runs over every couple of particles connected by a first-neighbor interaction; $\mathbf{u}_i = \mathbf{r}_i - \mathbf{R}_i$ is the displacement vector with respect to the rest position \mathbf{R}_i of particle i .

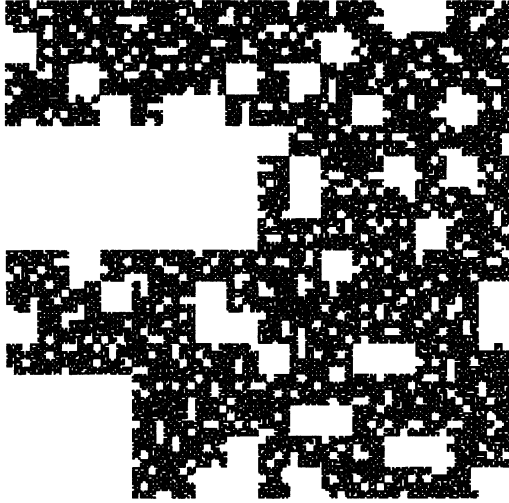


FIG. 1. Random Sierpinski carpet $C(4,13)$ at the iteration level $k = 4$.

Anyway, the random nature of structures we are dealing with makes numerical simulations necessary for a good study. The method used in order to derive the ground state under external stretch is the static relaxation process (SRP).^{17,18} The interest in such a method instead of molecular dynamics (MD) lies in the fact that the SRP enables us to determine in a complete and transparent way the elastic response of any network to a given external strain; moreover, the implementation of the SRP is much less heavy than MD. The computations carried out revealed that the elastic response of such networks to stretch is mainly determined by monodimensional structures. It implies a very particular behavior of the elastic bulk modulus. An analytical study of the monodimensional topological properties of two classes of networks is achieved: $R(n,q)$ and $C(n,p)$; it leads to a quantitative description in very good agreement with numerical results.

The existence of localized eigenstates plays a crucial role in the description of the vibrational properties of disordered materials; in the case of fractals, these localized modes have been called fractons¹⁹ by Alexander and Orbach. There has been a lot of work on these modes^{15,20} since fractons have been experimentally observed in silica aerogels. The study of the vibrational spectra of the networks we are dealing with reduces to that of longitudinal eigenstates, molecular modes, of a set of monodimensional structures; as already noted in studies on monodimensional disordered chains, these spectra show a very rich fine structure.²¹ Gaps appear in the density of states close to degenerate modes and could give a singular continuous^{13,22} character to some spectra. That spectral structure is completely determined by the length distribution of segments in the networks. Finally, a statistical formulation of the segmentation problem enabled us to find an analytical expression of the spectral distribution.

The organization of this paper is as follows: Section II deals with a description of the SRP and an analysis of numerical simulations. In Sec. III an analytical description of the behavior of the bulk elastic modulus in terms of

percolating straight lines is set out and compared with numerical results. Vibrational properties are discussed in Sec. IV for $R(n,q)$ and $C(n,p)$.

II. GENERALITIES: THE STATIC RELAXATION PROCESS

The SRP enables us to derive the equilibrium state of elastic networks when assuming given boundary conditions; the computing process occurs as follows.

(1) Boundary conditions are imposed by fixing the positions of given particles; for instance, in order to compute the elastic bulk modulus, particles at two opposite edges are moved along opposite directions, perpendicular to the edges with the same displacement δ .

(2) The elastic forces F_i exerted on each particle i are calculated.

(3) Every particle i , excepted the fixed ones, is allowed to relax with a displacement λF_i where λ is the relaxation parameter ($\lambda > 0$).

The two last steps are then reiterated in order to let each particle reach its equilibrium position; at each step N , the elastic energy $E(N)$ and the external forces exerted on the edges, $F_L(N)$ and $F_R(N)$, are calculated.

The choice of λ is crucial for the convergence: If λ is too large, the process does not allow the system to reach its equilibrium state. The energy decreases first until every particle has relaxed at least once and increases then at many relaxation steps to end with a chaotic oscillating behavior; for convenient temperature conditions, ultraslow relaxation phenomena²³ observed in gels present a similar behavior and will be studied separately. Since our purpose is to find the equilibrium state, the system has to be finally stationary with respect to the SRP, so that its energy and the external forces remain constant. It turns out from numerical simulations that we have then to choose $\lambda < 1/2k_e$. This limit value for λ and the nature of the relaxation process can be easily understood according to the following argument: Let us consider a particle placed between two springs linked to fixed points; if we call $\delta x(N)$ its displacement from equilibrium at the N th relaxation step, $\delta x(N+P)$ can be written $\delta x(N+P) = (1 - 2\lambda k_e)^P \delta x(N)$, a monotonous decrease of $\delta x(N)$ with the number of relaxation steps requires precisely $\lambda < 1/2k_e$. The SRP can be seen as a borderline case of MD with overdamping.¹⁸ Naturally, if λ is yet too low, the convergence is too slow and the number of steps we need to observe a stabilization of the energy is huge.

Numerical simulations have been carried out on random networks $R(n=16,q)$ and random Sierpinski carpets $C(n=4,p)$ at the second level of iteration ($k=2$); typical curves showing the evolution of the elastic energy $E(N)$ with the number of relaxation steps are reported in Fig. 2 with evidence for convergence with a distribution of effective relaxation times. Although the convergence is good, it turns out that even if the value of λ is optimized and the number of steps large, the equilibrium state seems to be still difficult to reach exactly. Since "relaxation times" are not distributed uniformly in the network because of its heterogeneity, there is a stretched re-

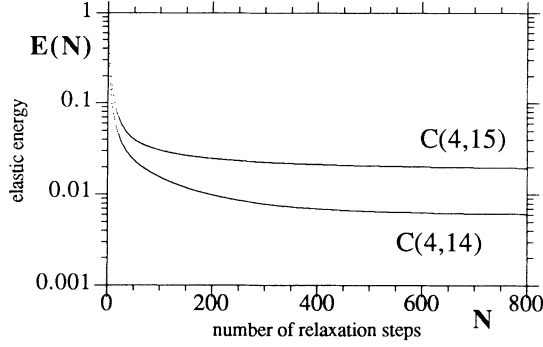


FIG. 2. Evolution of the elastic energy of the network against the number of relaxation steps in the case of two random Sierpinski carpets under stretching: $a=1$, $\delta=0.25$, $k_e=0.5$, and $\lambda=0.55$.

laxation at large N . A more precise analysis of the SRP leads to study a two-point elastic susceptibility²⁴ defined by the elastic response to the relative displacements of two particles in the network; it comes from numerical results that the elastic response has a significant value only if these two points are fully connected by a straight line and their displacements parallel to that line.

That last point can be understood from a development of H when analyzing the relative displacements $(\mathbf{u}_i - \mathbf{u}_j)$ into longitudinal and transverse components. Introducing the relative parallel displacement $(\mathbf{u}_i - \mathbf{u}_j)_\parallel$, which is the projection of the vector $(\mathbf{u}_i - \mathbf{u}_j)$ onto the vector $(\mathbf{R}_i - \mathbf{R}_j)$ at rest and of length a , the first nonconstant term in the series development of the total Hamiltonian H is quadratic in parallel displacements only:

$$\begin{aligned}
 H = & \frac{1}{2} k_e \sum (\mathbf{u}_i - \mathbf{u}_j)_\parallel^2 \\
 & + \frac{1}{2} k_e \sum \frac{(\mathbf{u}_i - \mathbf{u}_j)_\perp^2 \|(\mathbf{u}_i - \mathbf{u}_j)_\parallel\|}{a} \left[1 - \frac{\|(\mathbf{u}_i - \mathbf{u}_j)_\parallel\|}{a} \right] \\
 & + \frac{1}{2} k_e \sum \frac{(\mathbf{u}_i - \mathbf{u}_j)_\perp^4}{a^2}. \quad (2)
 \end{aligned}$$

$(\mathbf{u}_i - \mathbf{u}_j)_\perp$ is the transverse relative displacement. Three terms appear in the development of H :

$$H = H_\parallel^{(1)} + H_\perp^{(2)} + H_\perp^{(3)}. \quad (3)$$

$H_\parallel^{(1)}$, quadratic in parallel displacements, gives the linear part of the elastic response, $H_\perp^{(2)}$ expresses a coupling between transverse and longitudinal displacements, and $H_\perp^{(3)}$ is quartic in transverse displacements only. Considering two first neighbors occupying sites i and j , they define a line (ij) , and within $H_\parallel^{(1)}$ the parallel displacements $u_{i\parallel}, u_{j\parallel}$ are only coupled to the displacements $u_{k\parallel}$, where the site k belongs to the line (ij) and is connected with i or j by a full segment. In other words, in the harmonic approximation, i.e., $H_\parallel^{(1)}$, sites belonging to disconnected segments are not coupled.

The break of symmetry in the Hamiltonian between $(\mathbf{u}_i - \mathbf{u}_j)_\parallel$ and $(\mathbf{u}_i - \mathbf{u}_j)_\perp$ is found again during the relaxation process: Since the structure is submitted to a stretch, the main part of the information must be

transmitted parallel to the stretch direction. The elastic energy is dominated by $H_\parallel^{(1)}$, and the elastic response at low strain remains linear. The presence of unoccupied sites in the network locally induces inhomogeneity and elastic forces perpendicular to the stretch direction, leading to a transverse coupling expressed by $H_\perp^{(2)}$; that coupling is nonlinear and weak, since $H_\perp^{(2)}$ is one order of magnitude lower than $H_\parallel^{(1)}$. Thus the main part of the global elastic response of the network, i.e., bulk and shear moduli, is determined by geometric objects, the edge-to-edge percolating straight lines.

That conclusion clearly emerges from the whole set of numerical simulations we carried out, as in the following example: The displacement field of a random network $R(16,21)$ under a stretch parallel to the x direction after 4000 relaxation steps is shown in Fig. 3; the components of the external elastic forces \mathbf{F}_L and \mathbf{F}_R in the final state and the elastic energy calculated from the last step of the relaxation process are summarized in Table I. When the SRP is stopped, the relative variation of elastic energy from one step to the following one is less than 10^{-5} . The difference between the forces F_{Lx} and F_{Rx} and the nonzero residual value of the transverse components F_{Ly} and F_{Ry} express the existence of transverse coupling. Anyway, the relative difference between F_{Lx} and F_{Rx} is about $\frac{1}{1000}$, and the transverse forces remain about 1000 times smaller than the longitudinal ones; thus, to first order, the shear modulus is equal to zero.⁶ Moreover, the relative difference between the common value of F_{Lx} and F_{Rx} calculated from the assumption that the global elastic response is entirely due to the three percolating lines A, B, C noted in Fig. 3 and the numerical values of Table I is about 3%. Here 98% of the elastic energy of the net-

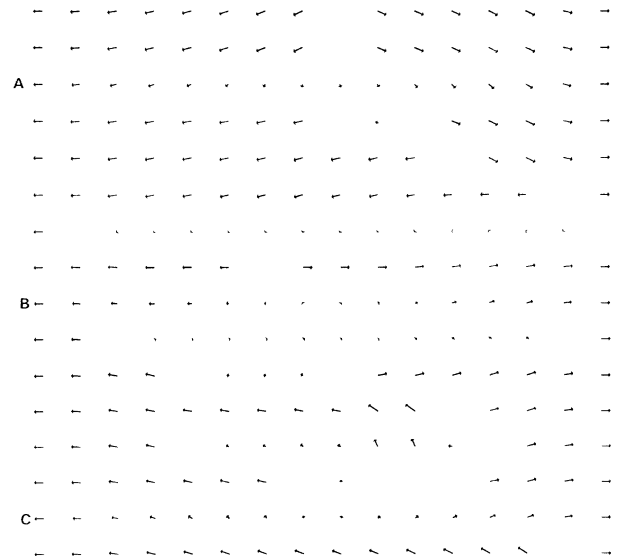


FIG. 3. Displacement field of a random network $R(16,21)$ under a stretch $\delta=0.25$ with $a=1$, $k_e=0.5$, and $\lambda=0.45$. Arrows represent local displacements of the particles between the network at rest and its distorted state; A, B, C are percolating lines.

TABLE I. Elastic energy and components of the elastic forces in the final state of a random network $R(16,21)$ calculated from the SRP after 4000 iteration steps. $\delta=0.25$, $a=1$; $k_e=0.5$, and $\lambda=0.45$.

F_{Lx}	F_{Rx}	F_{Ly}	F_{Ry}	E
0.051 763	-0.051 713	5.82×10^{-5}	-6.5×10^{-5}	0.012 658

work is localized along these lines. Otherwise, a fine observation of Fig. 3 shows that nonlinear effects expressed by $H_{\parallel}^{(2)}$ induce locally important transverse displacements, although the global elastic response remains determined by $H_{\parallel}^{(1)}$.

The behavior of the external forces F_L and F_R in the equilibrium state toward the displacement δ has been numerically studied in random networks $R(n,q)$ with $n=16$: Typical results collected in Fig. 4 prove that an elastic bulk modulus is defined without ambiguity for any given network, provided that it is dense enough.

On the other hand, a mean bulk modulus is defined for a given porosity, i.e., a given concentration of lacunas, by means of statistical treatment: The mean bulk modulus is directly proportional to the mean number of percolating straight lines. A very particular critical behavior of the mean bulk modulus as a function of density or fractal dimension is expected, since the elastic response at low strain is determined by a set of monodimensional structures—the percolating lines—for any dimension of the embedding space of the elastic network.

III. CRITICAL BEHAVIOR OF BULK MODULUS

A. Random networks $R(n,q)$

The mean number of percolating straight lines is analytically calculated by means of the generating function method²⁵ in the case of random spring networks $R(n,q)$ where $q \ll n^2$. Let us call $P_{n,q}(k)$ the probability that $(n-k)$ lines are percolating in a two-dimensional square network; i.e., k lines are cut. A recurrent relation

between the $P_{n,q}(k)$ can be found when considering the transition from $R(n,q)$ to $R(n,q+1)$ as a Markovian process. The existence of k cut lines after the introduction of an additional lacuna in $R(n,q)$ occurs in two different ways: Either there are k cut lines in the network $R(n,q)$ and the $(q+1)$ th lacuna is put in an already cut line or there are $(k-1)$ cut lines in $R(n,q)$ and the $(q+1)$ th lacuna is put in a percolating line. It gives then the probability $P_{n,q}(k)$, provided that $q \ll n^2$:

$$P_{n,q+1}(k) = \frac{k}{n} P_{n,q}(k) + \frac{n-k+1}{n} P_{n,q}(k-1), \quad (4)$$

with the normalization rule

$$\sum_{k=1}^n P_{n,q}(k) = 1.$$

This recurrent relation works only if $q \ll n^2$, since lines are assumed to be independently filled: The probability for a new lacuna to be put in an already cut line is taken as independent of the number of already present lacunas. The mean number $\langle M \rangle_{n,q}$ of percolating lines is then derived from the generating function $G_q(x) = \sum_{k=1}^n P_{n,q}(k)x^k$:

$$\langle M \rangle_{n,q} = n \left[\frac{n-1}{n} \right]^q. \quad (5)$$

This method gives also all the moments of the distribution of percolating lines and thus the fluctuations in this distribution.

A sharper analysis of the mean number of percolating lines is achieved when calculating first the probability $P(n,q)$ for a given line to be completely occupied:

$$P(n,q) = \frac{(n^2-n)!}{(n^2)!} \frac{(n^2-q)!}{(n^2-n-q)!}. \quad (6)$$

Assuming that $P(n,q)$ has the same value for every line, the mean number $\langle M \rangle_{n,q}$ is

$$\langle M \rangle_{n,q} = nP(n,q) = n \frac{(n^2-n)!}{(n^2)!} \frac{(n^2-q)!}{(n^2-n-q)!}. \quad (7)$$

An expansion of Eq. (7) using Stirling's formula,²⁶ provided that $n \ll n^2-q$ and $n \gg 1$, leads to the expression

$$\ln \left[\frac{\langle M \rangle_{n,q}}{n} \right] \approx -\frac{q}{n^2} \left[n + \frac{1}{2} + \frac{1}{2n} \right]. \quad (8)$$

It can be noted that the two approaches leading to Eqs. (5) and (7) are equivalent up to second order in the limit of large n , since they both lead to

$$\ln \left[\frac{\langle M \rangle_{n,q}}{n} \right] \approx -\frac{q}{n} \left[1 + \frac{1}{2n} \right]. \quad (9)$$

In order to check more precisely the validity of these approaches, a numerical study of the evolution of $\langle M \rangle_{n,q}$ with q has been done: For two given sizes ($n=16$ and 64) and for different values of q , the average $\langle M \rangle_{n,q}$ and its standard deviation are calculated from 300 different bidimensional networks; each network is constructed by using a trial process with a random number

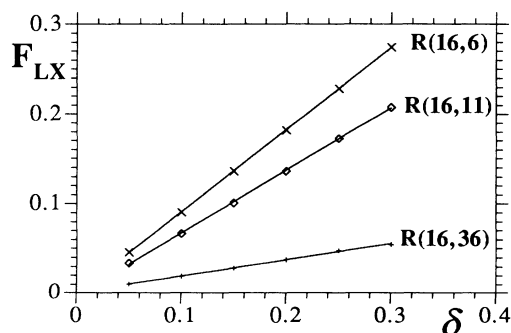


FIG. 4. Behavior of the component F_{Lx} of the external force vs displacement δ for three given networks; each point corresponds to the value of F_{Lx} calculated from the SRP. F_{Rx} is not plotted, since relative differences between F_{Lx} and F_{Rx} are always less than 2%.

generator. Figure 5 shows that exponential dependence of $\langle M \rangle_{n,q}$ upon q is well confirmed by numerical results provided that $\langle M \rangle_{n,q}$ is not too low; anyway, since fluctuations of order $1/\sqrt{300}$ are expected, because of the averaging process, small values of $\langle M \rangle_{n,q}$ are not meaningful. Moreover, theoretical predictions calculated from Eq. (8) lead to $\langle M \rangle_{16,q} = 15.5 \exp(-0.0647q)$ and $\langle M \rangle_{64,q} = 63.5 \exp(-0.0157q)$; it can be noted that the fit of $\langle M \rangle_{n,q}$ (working on 15 points) shown in Fig. 5 is in good agreement with these predictions.

The criterion for the critical elastic threshold is $\langle M \rangle_{n,q} = 1$ and enables us to define for each size (n) a linear percolation threshold, i.e., a critical number $q_c(n)$ of lacunas; the relative difference between the theoretical values calculated from Eq. (8) and the numerical values of the elastic threshold $q_c(n)$ are, respectively, about 4% for $n = 64$ and 6% for $n = 16$. Moreover, this difference lies within the accuracy of the averaging process; even if n is not very large, the linear percolation threshold $q_c(n)$ is given by $q_c(n) \approx n \ln(n)$, so that the critical density $d_c(n)$ is written as

$$d_c(n) \approx 1 - \frac{\ln(n)}{n} \tag{10}$$

In the macroscopic limit, when n tends to infinity the critical density tends to 1, as already noted above in the

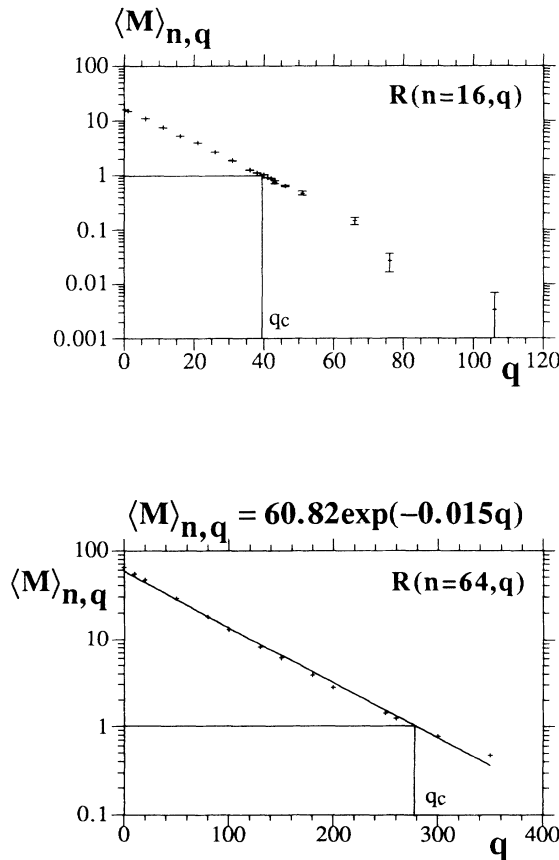


FIG. 5. Mean number of percolating lines vs number of lacunas q in the case of random networks $R(16, q)$ and $R(64, q)$; the fit shown below works only for meaningful values of q .

case of cubic lattices.⁶

The second analysis, leading to Eq. (7), is generalized to higher space dimensions $d > 2$: The mean number $\langle M \rangle_{n,q;d}$ of edge-to-edge percolating straight lines in a d -dimensional hypercubic random network with n^d sites and q lacuna is written as

$$\langle M \rangle_{n,q;d} = n^{d-1} \frac{(n^d - n)!}{(n^d)!} \frac{(n^d - q)!}{(n^d - n - q)!} \tag{11}$$

A Stirling's expansion²⁶ of $\langle M \rangle_{n,q;d}$ leads to

$$\ln \left[\frac{\langle M \rangle_{n,q;d}}{n^{d-1}} \right] \approx \left[-\frac{q}{n^d} \right] \left[n + \frac{n^2 - n}{2n^d} + \frac{2n^3 - n^2}{2(n^d)^2} \right] \tag{12}$$

So far that n is large enough, linear percolation can be more simply described by

$$\langle M \rangle_{n,q;d} \approx n^{d-1} \exp \left[-\frac{q}{n^{d-1}} \right] \tag{13}$$

The distribution of percolating monodimensional structures leads to the existence of an elastic threshold depending on the size of the network $q_c(n) \approx n^{d-1} \ln(n^{d-1})$ and to an exponential dependence of the bulk modulus upon the number of lacunas. In the macroscopic limit, the critical density tends to 1, as n tends to infinity for any space dimensionality $d > 1$:

$$d_c(n) \approx 1 - \frac{\ln(n^{d-1})}{n} \tag{14}$$

B. Random Sierpinski carpets $C(n, p)$

Two-dimensional random Sierpinski carpets contain random lacunary networks as basic elements in their hierarchical structure. A random Sierpinski carpet $C(n, p)$ where $n = 3, p = 7$ at the step $k = 2$ of iteration is shown in Fig. 6, where hatched squares of side a represent occupied sites. The mean number of percolating columns made up with squares of side na (bold framed ones) is $\langle M \rangle_{n,q}$ where $q = n^2 - p$; otherwise, the p squares of side $(n - 1)a$ are all independent, each square

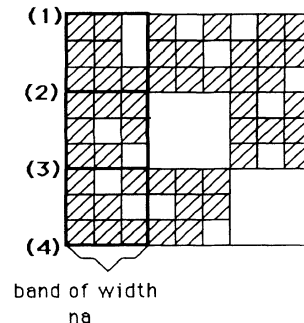


FIG. 6. Random Sierpinski carpet $C(3,7)$ at the iteration level $k = 2$.

TABLE II. Mean number of percolating lines in the case of random Sierpinski carpets $C(4,p)$, at different iteration levels k . Values calculated from numerical simulations are reported in the three left columns, theoretical ones in the three right columns; values less than 10^{-2} are not really observable because of fluctuations.

	$k=2$ (num.)	$k=3$ (num.)	$k=4$ (num.)	$k=2$ (theor.)	$k=3$ (theor.)	$k=4$ (theor.)
$p=15$	3.90	0.256	0	3.797	0.152	6.1×10^{-9}
$p=14$	0.93	0	0	0.805	0.0002	2.1×10^{-20}
$p=13$	0.22	0	0	0.149	1.9×10^{-7}	8.2×10^{-33}
$p=12$	0.024	0	0	0.0238	8.5×10^{-11}	1.1×10^{-38}

including $\langle M \rangle_{n,q}$ percolating lines so that the mean number $\langle \Phi \rangle_{n,p;k}$ of percolating lines can be written

$$\langle \Phi \rangle_{n,p;k=2} = \langle M \rangle_{n,q} \langle \hat{M} \rangle_{n,q},$$

where $\langle \hat{M} \rangle_{n,q}$ is the mean number of percolating lines inside a band of width na . The calculation of $\langle \hat{M} \rangle_{n,q}$ involves conditional probabilities linked to joins between squares of size na . Since the percolation of one line from edge (1) to edge (3) in Fig. 6 implies one coincidence among the n possible ones at the level of edge (2), the mean number of lines percolating from (1) to (3) is

$$\langle \hat{M} \rangle_{n,q}^{1 \rightarrow 3} = \langle M \rangle_{n,q} \frac{\langle M \rangle_{n,q}}{n};$$

a complete percolation implies $(n-1)$ such favorable joins, so that

$$\langle \hat{M} \rangle_{n,q} = \langle M \rangle_{n,q} \left[\frac{\langle M \rangle_{n,q}}{n} \right]^{n-1};$$

it comes down to, finally,

$$\langle \Phi \rangle_{n,p;k=2} = n^2 \left[\frac{C_{n^2-n}^{n^2-p}}{C_{n^2}^{n^2-p}} \right]^{(n^2+1)/(n-1)}, \quad (15)$$

where C_n^p is the binomial coefficient,²⁶

$$C_n^p = \binom{n}{p}.$$

This reasoning can be carried out further when studying the transition from step k to step $k+1$; there comes a recurrent relation between mean numbers $\langle \Phi \rangle_{n,p;k}$ and $\langle \Phi \rangle_{n,p;k+1}$ of percolating lines:

$$\langle \Phi \rangle_{n,p;k+1} = \langle M \rangle_{n,q} \langle \Phi \rangle_{n,p;k} \left[\frac{\langle \Phi \rangle_{n,p;k}}{n^{k-1}} \right]^{n-1}. \quad (16)$$

Finally, this recurrent relation (16) leads to

$$\langle \Phi \rangle_{n,p;k} = n^k \left[\frac{C_{n^2-n}^{n^2-p}}{C_{n^2}^{n^2-p}} \right]^{(n^{k+1})/(n-1)}. \quad (17)$$

Numerical simulations have been done in the case of random Sierpinski carpets $C(n,p)$, with $n=4$; the mean values $\langle \Phi \rangle_{n,p;k}$ have been calculated over 300 different $C(n,p)$. Numerical results at different steps of iteration k

are gathered in Table II and compared with theoretical ones calculated from Eq. (17).

The mean number of percolating lines, $\langle \Phi \rangle_{n,p;k}$, decreases very strongly with the number k of iteration steps; theoretical formula (17) gives a lower bound of the mean number of percolating lines, except for very low values of $\langle \Phi \rangle_{n,p;k}$, where fluctuations are too large to consider $\langle \Phi \rangle_{n,p;k}$ as meaningful. The reason for the difference between numerical and theoretical values can be understood when remarking that formula (17) is based on the assumption that mean values coincide with the most probable ones, what is an approximation for low n . Anyway, Fig. 7 shows that the exponential dependence of $\langle \Phi \rangle_{n,p;k}$ upon p , predicted by formula (17), is well obeyed by numerical results for $k=2$. On the other hand, in the macroscopic limit of large k , the bulk modulus of a bidimensional Sierpinski carpet is equal to zero.

IV. VIBRATIONAL PROPERTIES: THE SEGMENTATION PROBLEM

At first order, vibrational properties of random spring networks $R(n,q)$ and random fractals $C(n,p)$ are determined by longitudinal modes of monodimensional structures: independent segments. The transition between extended and localized modes can be defined by a percolation criterion: Phonons are associated with the edge-to-edge percolating straight lines, while molecular modes are localized along lines shorter than $(n-1)a$. Monodi-

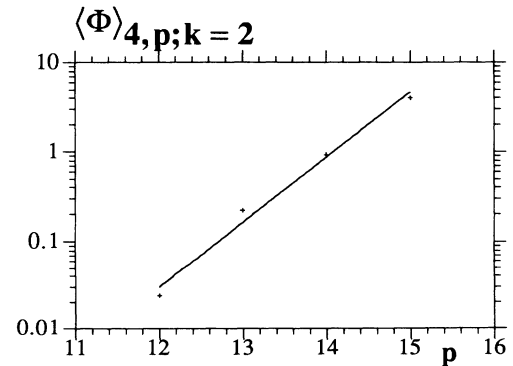


FIG. 7. Mean number of percolating lines as a function of p in the case of random Sierpinski carpets at the iteration level two with its fit.

dimensional vibrational states have been observed by Bourbonnais, Maynard, and Benoît¹⁵ in the case of deterministic Sierpinski carpets by means of MD and called "channeling modes."

The eigenvalues of the wave vector K , in the case of a monodimensional continuous linear chain with j sites, are given by $K = r\pi/(j-1)a$, with r varying from 1 to $(j-2)$. Computing the vibrational mode spectrum of a random network or a Sierpinski carpet reduces to a geometrical problem, counting up the number of segments with a given length.

A. Segmentation of random networks $R(n, q)$

The segmentation problem, i.e., the distribution in lines of length $(j-1)a$, is analytically solved in the case of two-dimensional random networks $R(n, q)$. Since q lacunas are distributed among n^2 sites, the size of the sample space is $C_{n^2}^q$. Two different cases must be considered when counting up the segments of length $(j-1)a$, parallel to a given direction (Δ), with $j < n$ as shown in Fig. 8.

(i) One tip is an edge of the network; a lacuna occurs at the $(j+1)$ th site in the line (A) and the other $(q-1)$ lacunas are distributed among the (n^2-j-1) remaining sites; the number of configurations containing that segment is $C_{n^2-j-1}^{q-1}$, there are n columns and two edges, so that the mean number of segments with length $(j-1)a$ and a tip at an edge is written as

$$\langle m(j) \rangle_{n,q}^{\text{edge}} = \frac{2nC_{n^2-j-1}^{q-1}}{C_{n^2}^q}. \quad (18)$$

(ii) The segment is limited by two unoccupied sites B

$$\langle m(j) \rangle_{n,q} = \frac{nC_{n^2-j-1}^{q-1} [2 + (q-1)(n-j-1)/(n^2-j-1)]}{C_{n^2}^q}. \quad (21)$$

A similar analysis leads to the mean number of percolating segments, as already studied in Sec. III, with the same result as Eq. (7):

$$\langle m(n) \rangle_{n,q} = \langle M \rangle_{n,q} = \frac{nC_{n^2-n}^q}{C_{n^2}^q}. \quad (22)$$

It has been ensured that $\langle m(j) \rangle_{n,q}$ satisfy the normalization rule

$$n \langle M \rangle_{n,q} + \sum_{j=1}^{n-1} j \langle m(j) \rangle_{n,q} = n^2 - q. \quad (23)$$

The expression (21) of $\langle m(j) \rangle_{n,q}$ is more easily compared to numerical results when using Stirling's formula.²⁶ The calculation leads to

$$\langle m(j) \rangle_{n,q} = \left[\frac{q}{n} \right] \left[1 - \frac{q}{n^2} \right]^j e^{\alpha j - \beta j^2 - \gamma j^3} \left\{ 2 + (q-1) \frac{n-j-1}{n^2-j-1} \right\}, \quad (24)$$

where

$$\alpha = \frac{2n^2 - q}{2n^2(n^2 - q)}, \quad \beta = \frac{q}{2n^2(n^2 - q)}, \quad \gamma = \frac{q(2n^2 - q)}{n^4(n^2 - q)^2}.$$

Numerical computations of the distributions

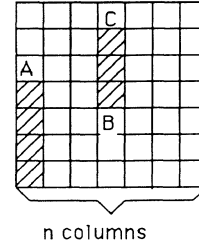


FIG. 8. Segmentation of a random network.

and C , which implies $j < (n-1)$; there is a lacuna in B , another one in C , and the $(q-2)$ remaining ones are distributed among n^2-j-2 sites, so that there are $C_{n^2-j-2}^{q-2}$ configurations containing that segment; since there are $(n-j-1)$ different possible positions in that column (BC) and n columns, the mean number of segments with a length $(j-1)a$ and an unoccupied site at each tip is written as

$$\langle m(j) \rangle_{n,q}^{\text{bulk}} = \frac{n(n-j-1)C_{n^2-j-2}^{q-2}}{C_{n^2}^q}. \quad (19)$$

Finally, the mean number of segments of length $(j-1)a$ is

$$\langle m(j) \rangle_{n,q} = \frac{2nC_{n^2-j-1}^{q-1} + n(n-j-1)C_{n^2-j-2}^{q-2}}{C_{n^2}^q}. \quad (20)$$

This expression of $\langle m(j) \rangle_{n,q}$ works for j running from 1 to $(n-1)$ included, since the second term vanishes when $j = n-1$; $\langle m(j) \rangle_{n,q}$ can also be written

$\langle m(j) \rangle_{n,q}$ have been carried out in the same way as the study of $\langle M \rangle_{n,q}$: For a given size (n) and a given concentration (q/n^2), the mean values $\langle m(j) \rangle_{n,q}$ (with $0 < j < n$) and their standard deviations have been calculated from a statistics over 300 random networks; more precisely, we considered 15 different values of q , between

6 and 150 in the case $n = 16$, and 20 different values of q , between 10 and 1500 in the case $n = 64$. The main results are summarized in Fig. 9; error bars $(\Delta m(j))_{n,q}$ have been calculated in the framework of the normal approximation:²⁵

$$(\Delta m(j))_{n,q} = \left[\frac{\langle m^2(j) \rangle_{n,q} - [\langle m(j) \rangle_{n,q}]^2}{300} \right]^{1/2}. \quad (25)$$

Since α, β, γ are small and j is varying only from 1 to n , theoretical points have been calculated from a simplified form of the analytical expression of $\langle m(j) \rangle_{n,q}$:

$$\langle m(j) \rangle_{n,q} \approx \left[\frac{q}{n} \right] \left[1 - \frac{q}{n^2} \right]^j \left[2 + (q-1) \frac{n-j-1}{n^2-j-1} \right]. \quad (26)$$

The use of formula (26) instead of (24) is justified from an analysis of the fluctuations of $\langle m(j) \rangle_{n,q}$: The agreement between numerical results and the analytical law can be precisely studied here, since statistical fluctuations $[(\Delta m(j))_{n,q} / \langle m(j) \rangle_{n,q}]_{\text{num}}$ of $\langle m(j) \rangle_{n,q}$ can be compared with the difference between numerical and analytical results. Table III shows the average $\langle \Delta m / m \rangle_{\text{num}}$ of $[(\Delta m(j))_{n,q} / \langle m(j) \rangle_{n,q}]_{\text{num}}$ calculated over the $(n-1)$ numerical values of j and the average relative differences $\langle \Delta m / m \rangle_{\text{diff}}$ between numerical and theoretical values.

The difference between numerical and theoretical values lies within the range of statistical fluctuations. The length distribution is rather flat for small values of q , and so fluctuations are almost not dependent on j , whereas they are important at large j when q is larger.

The segmentation problem is generalized to any space dimensionality d larger than 2; the mean number $\langle m(j) \rangle_{n,q;d}$ of monodimensional segments of length $(j-1)a$ ($j < n$) in a d -dimensional hypercubic random network with n^d sites and q lacuna is written as

$$\langle m(j) \rangle_{n,q;d} = \frac{2n^{d-1} C_{n^d-j-1}^{q-1} + n^{d-1}(n-j-1) C_{n^d-j-2}^{q-2}}{C_{n^d}^q} \quad (j < n), \quad (27)$$

where the first term is associated with the segments adjacent to the edges and the second term with bulk segments; $\langle m(j) \rangle_{n,q;d}$ is expanded using Stirling's formula²⁶ in the same way as in the two-dimensional case, so that

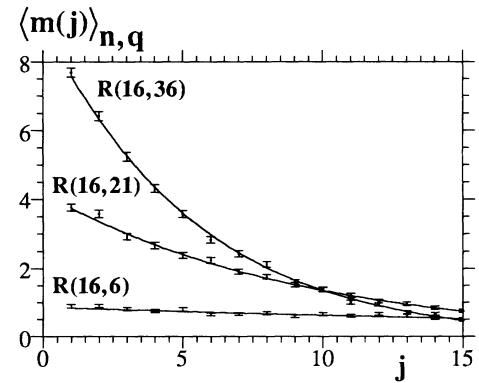
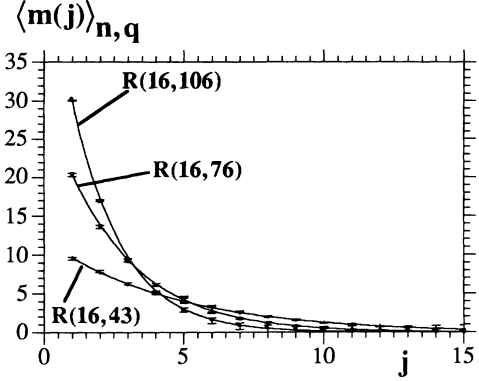


FIG. 9. Distribution in lengths in random networks $R(16, q)$. Points resulting from numerical computations are represented by dots; solid curves show theoretical fits calculated from Eq. (26).

segmentation is finally given by

$$\langle m(j) \rangle_{n,q;d} = \left[\frac{q}{n} \right] \left[1 - \frac{q}{n^d} \right]^j e^{\alpha j - \beta j^2 - \gamma j^3} \times \left[2 + (q-1) \frac{n-j-1}{n^d-j-1} \right], \quad (28)$$

where

$$\alpha = \frac{2n^d - q}{2n^d(n^d - q)}, \quad \beta = \frac{q}{2n^d(n^d - q)}, \quad \gamma = \frac{q(2n^d - q)}{n^{2d}(n^d - q)^2}.$$

TABLE III. Averages $\langle \Delta m / m \rangle_{\text{num}}$ of the relative fluctuations of $\langle m(j) \rangle_{n,q}$ calculated from numerical simulations, compared with the mean relative differences $\langle \Delta m / m \rangle_{\text{diff}}$ between theoretical and numerical values, for different random networks $R(n, q)$.

	$R(16, 6)$	$R(16, 21)$	$R(16, 36)$	$R(16, 43)$	$R(16, 76)$	$R(64, 20)$	$R(64, 130)$	$R(64, 600)$
$\langle \frac{\Delta m}{m} \rangle_{\text{diff}}$	0.053	0.021	0.033	0.046	0.073	0.074	0.041	0.2
$\langle \frac{\Delta m}{m} \rangle_{\text{num}}$	0.066	0.043	0.043	0.047	0.085	0.077	0.043	0.2

B. Segmentation of random Sierpinski carpets $C(n, p)$

The hierarchical structure of Sierpinski carpets makes their segmentation problem rather different from that for random networks $R(n, q)$. The main features of the length distribution in $C(n, p)$ appear in the transition from a step k of iteration to the following one. Let us call $\langle \varphi(j) \rangle_{n,p;k}$ the mean number of segments of length $(j-1)a$, parallel to a given direction (Δ) in a random Sierpinski carpet $C(n, p)$ at the step k ; this number splits into an edge component $\langle \varphi(j) \rangle_{n,p;k}^e$, including every segment with a tip at an edge, and a "bulk" one $\langle \varphi(j) \rangle_{n,p;k}^b$. Since there are p subsquares of size $(n^k-1)a$ in a Sierpinski carpet at the step $(k+1)$ of iteration, $\langle \varphi(j) \rangle_{n,p;k+1}$ are deduced from $\langle \varphi(j) \rangle_{n,p;k}$ when analyzing coin-

cidences between segments belonging to different adjacent subsquares along their common edge; the only connections between subsquares we consider in the following refer to the direction (Δ).

Different cases must be distinguished according to the segment length.

(i) If $1 < j < n^k$, a segment of this length belongs to one among three categories: Either this segment occurs in the bulk of a subsquare, it occurs at an edge of a subsquare without connection with another one, or it results from a coincidence between two segments of lengths j_1 and $j-j_1$ located in occupied adjacent subsquares. Calling $\langle c \rangle_{n,q}$ the mean number of connections between subsquares of size n^k , the recurrent relation is written as a sum of three terms corresponding, respectively, to the three cases described above:

$$\langle \varphi(j) \rangle_{n,p;k+1} = p \langle \varphi(j) \rangle_{n,p;k}^b + [n(n-1) - \langle c \rangle_{n,q}] \langle \varphi(j) \rangle_{n,p;k}^e + \frac{\langle c \rangle_{n,q}}{4n^k} \sum_{i=0}^{i=j} \langle \varphi(i) \rangle_{n,p;k}^e \langle \varphi(j-i) \rangle_{n,p;k}^e, \tag{29}$$

where $\langle c \rangle_{n,q} = \sum_{i=1}^{i=n} (i-1) \langle m(i) \rangle_{n,q}$ is expressed in terms of the length distribution in the random subnetwork $R(n, q)$ made up with subsquares of size n^k ($p = n^2 - q$).

(ii) If $j = n^k$, four different origins must be considered for such a long segment: It can be already present in an isolated subsquare, in a subsquare connected with another one, in a subsquare connected with two others, or result from a coincidence. Calling $\langle c1 \rangle_{n,q} = \sum_{i=2}^{i=n} \langle m(i) \rangle_{n,q}$ the mean number of subsquares connected once and $\langle c2 \rangle_{n,q} = \sum_{i=2}^{i=n} (i-2) \langle m(i) \rangle_{n,q}$ the mean number of subsquares connected twice, the recurrent relation can be written

$$\begin{aligned} \langle \varphi(j) \rangle_{n,p;k+1} = & \langle \varphi(j) \rangle_{n,p;k} \langle m(1) \rangle_{n,q} + \langle c1 \rangle_{n,q} \frac{\langle \varphi(0) \rangle_{n,p;k}^e \langle \varphi(n^k) \rangle_{n,p;k}}{n^k} \\ & + \frac{\langle c \rangle_{n,q}}{4n^k} \sum_{i=1}^{i=n^k-1} \langle \varphi(i) \rangle_{n,p;k}^e \langle \varphi(j-i) \rangle_{n,p;k}^e + \langle c2 \rangle_{n,q} \left[\frac{\langle \varphi(0) \rangle_{n,p;k}^e}{2n^k} \right]^2 \langle \varphi(n^k) \rangle_{n,p;k}. \end{aligned} \tag{30}$$

(iii) If $n^k + 1 < j < 2n^k$, the segment has three possible origins: Either it results from a single coincidence between a segment of length n^k belonging to a subsquare placed at a tip of a subsegment and a segment of length $j - n^k$, it results from a coincidence between two segments of lengths j_1 and j_2 , or it is built in three parts. The recurrent relation is written as

$$\begin{aligned} \langle \varphi(j) \rangle_{n,p;k+1} = & \langle c1 \rangle_{n,q} \langle \varphi(n^k) \rangle_{n,p;k} \frac{\langle \varphi(j-n^k) \rangle_{n,p;k}^e}{n^k} + \frac{\langle c \rangle_{n,q}}{4n^k} \sum_{i=0}^{i=j} \langle \varphi(i) \rangle_{n,p;k}^e \langle \varphi(j-i) \rangle_{n,p;k}^e \\ & + \langle c2 \rangle_{n,q} \frac{\langle \varphi(n^k) \rangle_{n,p;k}}{4(n^k)^2} \sum_{i=0}^{i=n^k-j} \langle \varphi(i) \rangle_{n,p;k}^e \langle \varphi(j-n^k-i) \rangle_{n,p;k}^e. \end{aligned} \tag{31}$$

Curves showing the behavior of $\langle \varphi(j) \rangle_{n,p;k}$, obtained from numerical computations, according to the same procedure as $\langle m(j) \rangle_{n,q}$ are reported in Fig. 10. It can be noted that $\langle \varphi(j) \rangle_{n,p;k}$ exhibits an oscillatory behavior with a periodicity $n=4$ superposed on a mean exponential; oscillations occurring at very low values of $\langle \varphi(j) \rangle_{n,p;k}$ are not meaningful because of fluctuations; the decrease of $\langle \varphi(j) \rangle_{n,p;k}$ when j goes from αn to $\alpha n + 1$, with α integer and $0 < \alpha < n^k$, can be understood when considering the differences between the recurrent relations (30) and (31). On the one hand, the first term in relation (30) gives no more contribution in relation (31); on the other hand, the lengthening of j by one unit involves an additional coincidence. Oscillations become

smoother when p decreases because $\langle c \rangle_{n,q}$, $\langle c1 \rangle_{n,q}$, and $\langle c2 \rangle_{n,q}$ tend to zero. High values of j are strongly disadvantaged when k increases, while involving products of a great number of conditional probabilities.

C. Vibrational spectra

Vibrational spectra associated with longitudinal modes of monodimensional structures are deduced from length distributions.

In the case of random networks $R(n, q)$, the mean number $\langle N(K) \rangle_{n,q}$ of modes with a wave vector $K = r\pi/(j-1)a$ localized along segments shorter than $(n-1)a$ can be written

$$\langle N(K) \rangle_{n,q} = \sum_{j=3}^{j=n-1} g_{j,K} \langle m(j) \rangle_{n,q}, \quad (32)$$

where $g_{j,K} = 1$ if the segment with a length $(j - 1)a$ contributes to a mode of wave vector K and $g_{j,K} = 0$ otherwise.

The set of wave vector eigenvalues is classified in a more useful way: It is always possible to write $K(n_1, n_2) = (\pi/a)(n_1/n_2)$, where (n_1/n_2) is an irreduc-

ible fraction with $n_1 < n_2$ and n_2 runs from 1 to $(n - 2)$ included; $g_{j,K}(n_1, n_2)$ is then different from zero if there is an integer r so that $r = (j - 1)(n_1/n_2)$, with $(r < j - 1)$. The number of different lengths which contribute to the same mode $K(n_1, n_2)$ defines the degeneracy $g(K(n_1, n_2))$ of the mode $K(n_1, n_2)$:

$$g(K(n_1, n_2)) = \sum_j g_{j,K}. \quad (33)$$

The set of values taken by $g(K(n_1, n_2))$ depends on the size of the network; when dealing with localized modes, j runs only from 3 to $(n - 1)$ included. Thus $g(K(n_1, n_2))$ is written as

$$g(K(n_1, n_2)) = E \left[\frac{n - 2}{n_2} \right], \quad (34)$$

where $E(x)$ is the integer part of x ; n_2 runs from 2 to $(n - 2)$ included. Several authors, dealing with excitation spectra in deterministic Sierpinski gaskets,^{12,14} noted

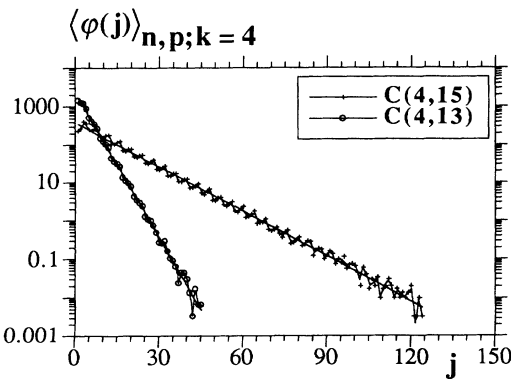
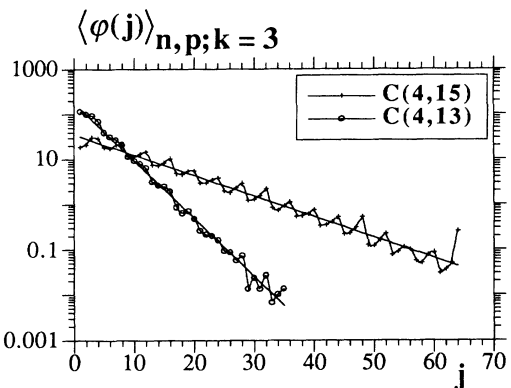
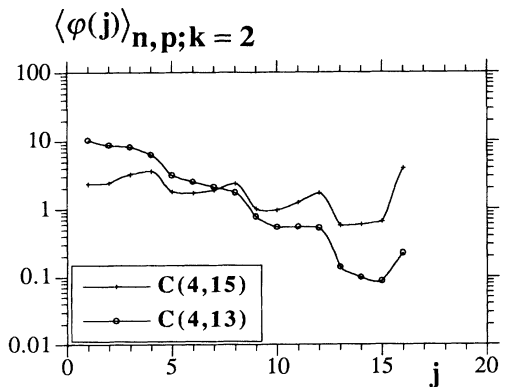


FIG. 10. Distribution in lengths in random Sierpinski carpets at different iteration levels. Points resulting from numerical computations are represented by dots and linked by solid curves. Straight lines drawn in the cases $k = 3$ and 4 are calculated from exponential fits.

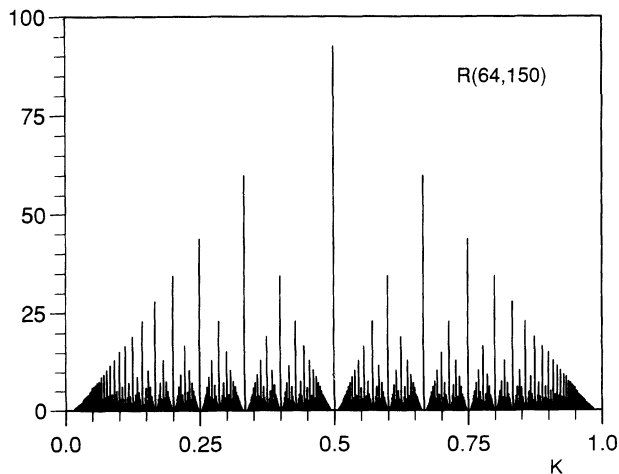
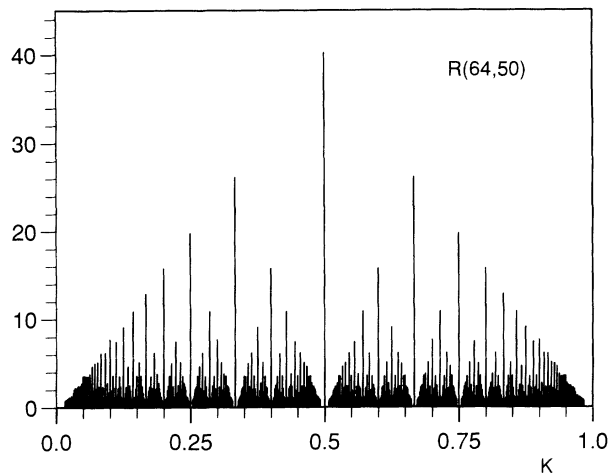


FIG. 11. Vibrational spectra of random networks $R(64, q)$ above the linear percolation threshold $q_c(64) = 266$; $\langle N(K) \rangle_{n,q}$ is plotted as a function of K in (n_1/n_2) units.

such an effect of mode degeneracy, which is here understood as a geometrical effect.

Spectra have been computed from numerical simulations according to the same process as described in Sec. IV A; typical results are reported in Figs. 11 and 12, where the mean values $\langle N(K) \rangle_{n,q}$ are plotted versus (n_1/n_2) ; modes associated with percolating lines are not taken into account. Since the degeneracy $g(K(n_1, n_2))$ is not dependent on n_1 , spectra are symmetric with respect to the mode $(n_1/n_2) = \frac{1}{2}$. As long as the number of lacunas is low, the length distribution remains rather flat and all modes are present in the spectrum, with an intensity proportional to their degeneracy. Peaks corresponding to modes $K(1, n_2)$ line up along a straight line of slope s ; peaks corresponding to modes $K(2, n_2)$ line up along another straight line with a slope $s/2$, and so on.

The distribution $\langle m(j) \rangle_{n,q}$ exhibits an exponential outline all the more marked than when q is increased, so that long segments become quite scarce; the intensities of modes associated with long segments decrease when q is increased, all the more quickly than when their degenera-

cy is low, until they disappear. So gaps appear at the feet of highly degenerate modes as seen in Figs. 11 and 12.

The behavior at low q is well discriminated from the one at large q when plotting the integrated density of states (IDOS) in K : Figure 13 shows such graphs, where the total mean number of states, $\langle N_I(K) \rangle_{n,q}$, with a wave vector lower than K is plotted in units (n_1/n_2) ; the profile of $\langle N_I(K) \rangle_{n,q}$ is well known as a devil's staircase.²² The width of gaps located at $(n_1/n_2) = \frac{1}{2}$ is larger than at $(n_1/n_2) = \frac{1}{3}$ and more generally decreases with n_2 . Furthermore, both gap widths and intensities of degenerate modes increase when q is increased.

When the total measure of gaps tends towards 1, the spectrum becomes by definition singular continuous;²⁷ this appears in the macroscopic limit when long segments become unimportant, i.e., near the linear percolation threshold. For larger lacuna concentrations, only finite segments occur, and there is a discrete Dirac spectrum of singularities.

In the case of random Sierpinski carpets, the mean number $\langle \nu(K) \rangle_{n,p;k}$ of modes with a wave vector K is

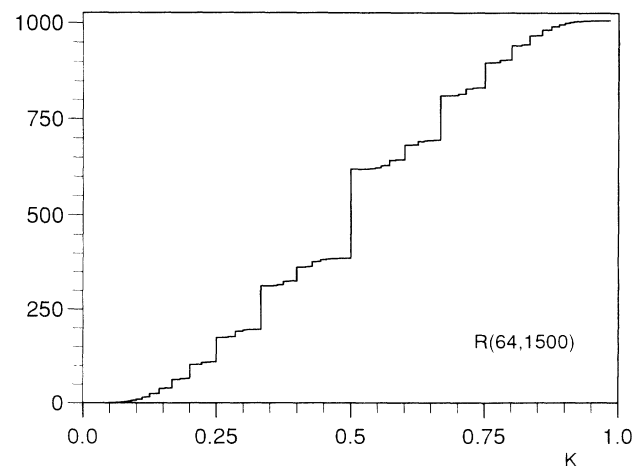
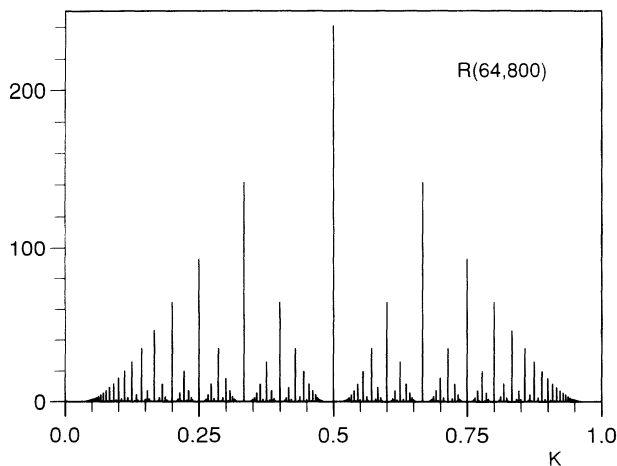
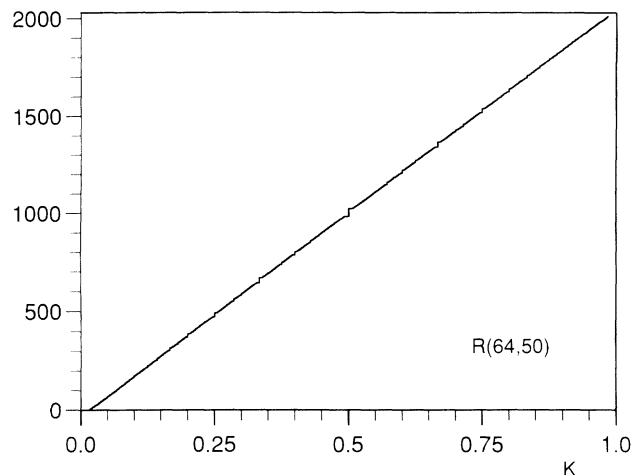
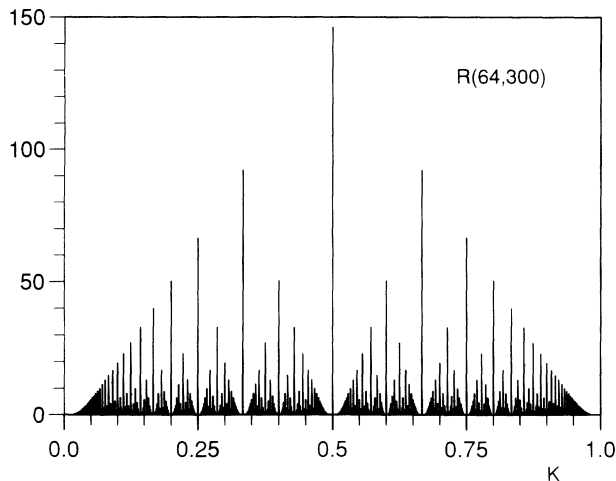


FIG. 12. Vibrational spectra of random networks $R(64, q)$ below the linear percolation threshold $q_c(64) = 266$; $\langle N(K) \rangle_{n,q}$ is plotted as a function of K in (n_1/n_2) units.

FIG. 13. Integrated density of states (IDOS) in K for two random networks $R(64, q)$; $\langle N_I(K) \rangle_{n,q}$ is plotted vs K in (n_1/n_2) units.

written as

$$\langle \nu(K) \rangle_{n,p;k} = \sum_{j=3}^{j=n^k-1} g_{j,K} \langle \varphi(j) \rangle_{n,p;k} . \quad (35)$$

Spectra calculated from numerical computations are shown in Fig. 14. They reflect the oscillatory behavior of $\langle \varphi(j) \rangle_{n,p;k}$: Since segments with lengths $4ra$, with r integer, are disadvantaged, the intensities of modes such as $(n_1/n_2)=1/4r$ are weakened in comparison with that for random networks $R(n,q)$. It is clearer when p is large, since oscillations become larger, as already noted before; that effect is seen from comparison between Figs. 14(a) and 14(b). The IDOS plotted in Fig. 15 shows gaps appearing in the spectrum²² close to degenerate modes; their widths decrease as expected when p increases. Since segmentation on random Sierpinski carpets emphasizes short lengths when k increases, their spectrum is always discrete in the infinite limit.

In a concluding remark, it must be noted that the elastic decoupling in independent segments neglects anharmonic contributions from central forces, so that the ap-

proximation is strictly valid only at low strains and at low vibrational intensities. In the case of large strains or large vibrational intensities, transverse coupling occurs, and there is not a perfect pinning of vibrational modes at elbows and angles. From that point of view, the pioneering work of Bourbonnais, Maynard, and Benoît on MD in deterministic Sierpinski carpets proved the existence of channeling modes,¹⁵ i.e., that propagation is restricted to full segments; it is a proof of the efficiency of the harmonic approximation by means of MD computations. Of course, the introduction of anharmonic coupling involves the contribution of elbows in the segmentation process. Similar remarks also apply to composite materials where sites of the network are filled with particles A and lacunas replaced by another kind of material particles B . In such composites, previous calculations remain valid in the weak-coupling limit between particles A and B , and basic effects are due to separate matrices A and B only. Finally, the geometrical part of percolation in the appearance of singular continuous spectra is general and easy to understand. For finite n , below the percolation threshold, there are only finite clusters⁵ and thus a finite set of

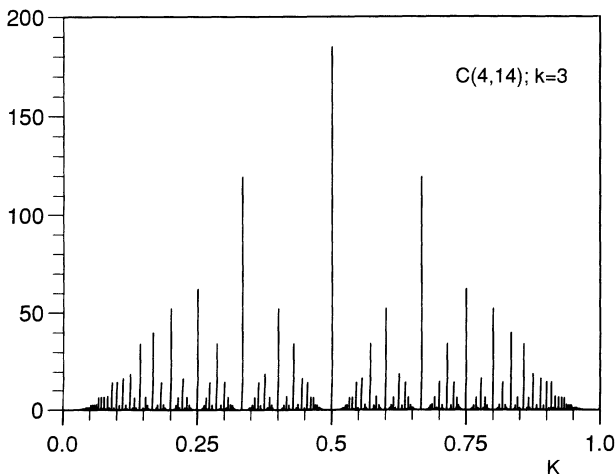
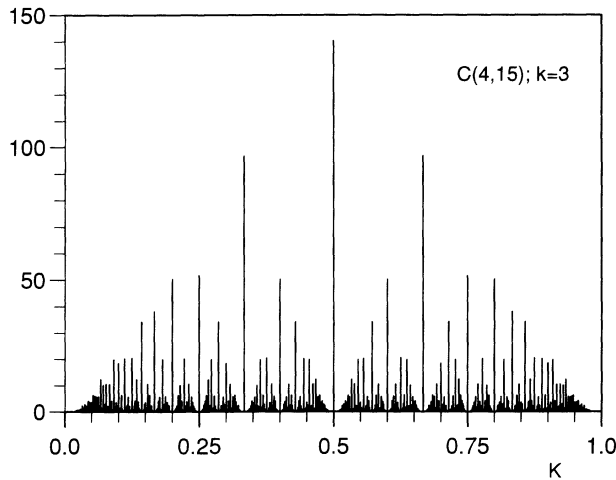


FIG. 14. Vibrational spectra of random Sierpinski carpets $C(4,p)$ at the iteration level $k=3$; $\langle \nu(K) \rangle_{n,p;k}$ is plotted as a function of K in (n_1/n_2) units.

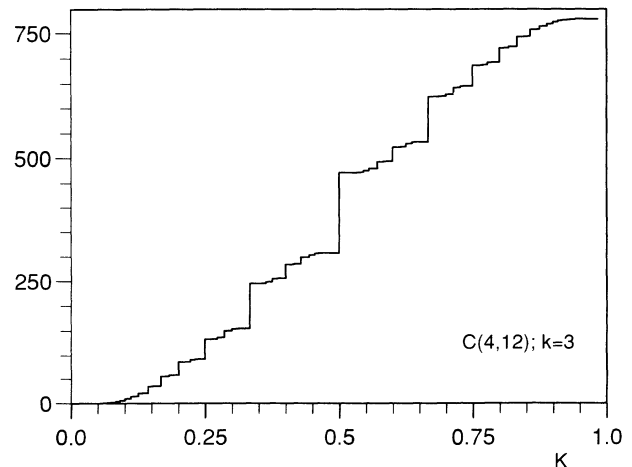
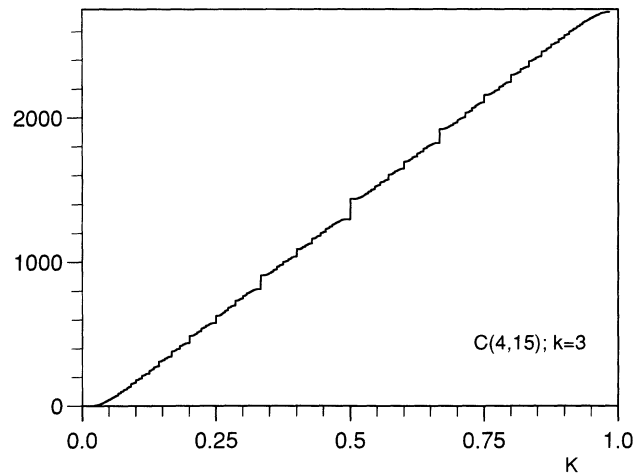


FIG. 15. Integrated density of states (IDOS) in K for two random Sierpinski carpets $C(4,p)$ at the iteration level $k=3$; K is in (n_1/n_2) units.

Dirac peaks in the excitation spectrum except near the percolation threshold. Above the percolation threshold, the distribution of finite clusters decreases exponentially⁵ and the excitation spectrum becomes dominated by bulk

excitations, i.e., phonons. Since the percolation arguments developed in Ref. 5 are valid for bond percolation and are quite general, singular continuous spectra can occur only at the vicinity of percolation thresholds.

-
- ¹H. E. Stanley, *Disordered Systems and Localization*, Lecture Notes in Physics Vol. 149 (Springer-Verlag, Berlin, 1981).
- ²*Composite Materials*, edited by A. T. Di Benedetto, L. Nicolais, and R. Watanabe (Elsevier, Amsterdam, 1992).
- ³P. G. De Gennes, *J. Phys. (Paris) Lett.* **37**, L1 (1976).
- ⁴Y. Kantor and I. Webman, *Phys. Rev. Lett.* **52**, 1891 (1984).
- ⁵G. Grimmett, *Percolation* (Springer-Verlag, New York, 1989).
- ⁶S. Feng and P. N. Sen, *Phys. Rev. Lett.* **52**, 216 (1984).
- ⁷M. Born and K. Huang, *Dynamical Theory of Crystal Lattices* (Oxford University Press, New York, 1954).
- ⁸E. J. Garboczi and M. F. Thorpe, *Phys. Rev. B* **31**, 7276 (1985).
- ⁹A. Hansen, in *Statistical Models for the Fracture of Disordered Media*, edited by H. J. Herrmann and S. Roux (Elsevier, Amsterdam, 1990), p. 115.
- ¹⁰E. Duering and D. J. Bergman, *Physica A* **157**, 561 (1989).
- ¹¹D. J. Bergman and Y. Kantor, *Phys. Rev. Lett.* **53**, 511 (1984).
- ¹²E. Domany, S. Alexander, D. Bensimon, and L. P. Kadanoff, *Phys. Rev. B* **28**, 3110 (1983).
- ¹³R. Rammal, *J. Phys. (Paris) Lett.* **45**, 191 (1984).
- ¹⁴U. Sivan, R. Blumenfeld, Y. Meir, and O. Entin-Wohlman, *Europhys. Lett.* **7**, 249 (1988).
- ¹⁵R. Bourbonnais, R. Maynard, and A. Benoît, *J. Phys. (Paris)* **50**, 3331 (1989).
- ¹⁶Y. Gefen, A. Aharony, Y. Shapir, and B. B. Madelbrot, *J. Phys. A* **17**, 435 (1984); **17**, 1277 (1984).
- ¹⁷D. Mercier and J. C. S. Levy, *Phys. Rev. B* **27**, 1293 (1983).
- ¹⁸J. Roth, R. Schilling, and H. R. Trebin, *Phys. Rev. B* **41**, 2735 (1990).
- ¹⁹S. Alexander and R. Orbach, *J. Phys. (Paris) Lett.* **43**, L625 (1982).
- ²⁰E. Courtens, J. Pelous, J. Phalippou, R. Vacher, and T. Woignier, *Phys. Rev. Lett.* **58**, 128 (1987).
- ²¹W. M. Visscher and J. E. Gubernatis, in *Dynamical Properties of Solids*, edited by G. K. Horton and A. A. Maradudin (Elsevier, Amsterdam, 1980), Vol. 4, p. 63.
- ²²J. M. Luck, *Phys. Rev. B* **39**, 5834 (1989).
- ²³T. Dorfmueller and J. Stellbrink, *Ber. Bunsenges. Phys. Chem.* **95**, 1100 (1991).
- ²⁴J. Wang and A. Brooks Harris, *Phys. Rev. B* **40**, 7272 (1989).
- ²⁵W. Feller, *An Introduction to Probability Theory and Its Applications* (Wiley, New York, 1970), Vol. I.
- ²⁶*Handbook of Mathematical Functions*, edited by M. Abramowitz and I. A. Stegun (N.B.S., Washington, D.C., 1964).
- ²⁷E. C. Titchmarsh, *The Theory of Functions*, 2nd ed. (Oxford University Press, New York, 1979).

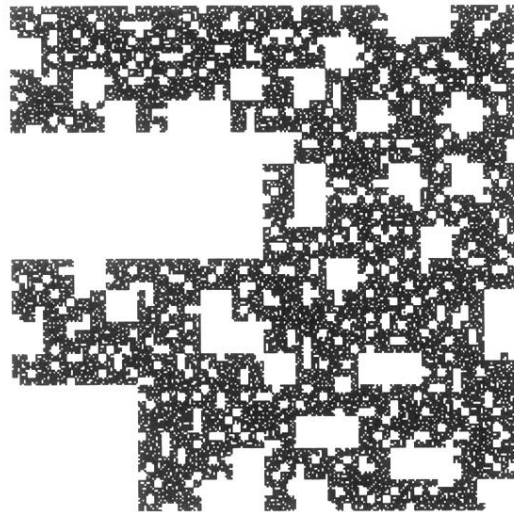


FIG. 1. Random Sierpinski carpet $C(4,13)$ at the iteration level $k = 4$.